Excited states and photodissociation dynamics of the triiodine radical (I_3)

Hyeon Choi[a)]
Department of Chemistry, University of California, Berkeley, California 94720 and Chemical Sciences Division, Lawrence Berkeley National Laboratory, Berkeley, California 94720

Travis R. Taylor[b)]
Lam Research, A7131 Bayside Parkway, Fremont, California 94538-6517

Ryan T. Bise
Lucent Technologies, Room 7C-227, 600-700 Mountain Avenue, Murray Hill, New Jersey 07974

Alexandra A. Hoops and Daniel M. Neumark
Department of Chemistry, University of California, Berkeley, California 94720 and Chemical Sciences Division, Lawrence Berkeley National Laboratory, Berkeley, California 94720

(Received 13 June 2000; accepted 24 August 2000)

The electronic spectroscopy and photodissociation dynamics of the I_3 radical are investigated with two experimental methods. The ground and several low-lying excited states of the I_3 radical are characterized by photoelectron spectroscopy of I_3^- at 213 nm. Assignments of these states are discussed with reference to recent calculations. In addition, photodissociation of the I_3 radical was investigated at selected photon energies (4.59, 4.96, and 5.17 eV) by fast radical beam photofragment translational spectroscopy. Two product channels were observed with mass ratios of 1:2 and 1:1, and translational energy ($P(E_T)$) distributions were measured. The $P(E_T)$ distributions for products with mass ratio 1:2 show that this channel corresponds to I_2 in various electronic states along with atomic I in its $^2P_{3/2}$ or $^2P_{1/2}$ state. The 1:1 channel corresponds primarily to concerted three-body dissociation to three I atoms. © *2000 American Institute of Physics.* [S0021-9606(00)01043-6]

I. INTRODUCTION

The triiodine radical (I_3) has been proposed to be a key intermediate in the iodine atom recombination reaction $I+I \rightarrow I_2$,[1] and in the conversion between ortho- and para-I_2 through $I+I_2$ complex-forming collisions.[2] The existence of stable excited states of the I_3 radical has been postulated to explain the efficient quenching of $I^*(^2P_{1/2})$ by I_2,[3–5] a process of interest in iodine chemical lasers. However, only recently has the I_3 radical been experimentally observed and shown to have a stable ground state,[6] while considerably less is known about the excited states of I_3. In this work, we use a combination of photoelectron spectroscopy and photofragment translational spectroscopy to further elucidate the ground state of I_3 and to probe the spectroscopy and dynamics of its excited electronic states.

To date, the only direct experimental observation of I_3 comes from photoelectron spectroscopy (PES) of I_3^-. The PES spectrum of I_3^- by Taylor *et al.*[6] at a photodetachment wavelength of 266 nm yielded the electron affinity of I_3, 4.226 ± 0.013 eV. This value in conjunction with the dissociation energy of I_3^- measured by Sunderlin and co-workers[7] showed that I_3 was stable by 0.14 eV with respect to dissociation to $I+I_2$. The photoelectron spectrum showed a low-frequency vibrational progression (115 ± 5 cm^{-1}) in the I_3 ground state that was assigned to the symmetric stretch, and simulations of the spectrum suggested the I_3 ground state to be linear and centrosymmetric. The PES showed that there was an excited state of I_3 0.27 eV above the ground state. A lower resolution, two-photon PES of I_3^- taken by Zanni *et al.*[8,9] using femtosecond laser pulses at 390 nm showed evidence for higher excited states of I_3 lying 0.68 and 1.48 eV above the ground state.

No assignments of the I_3 electronic states were proposed in these photoelectron studies. Since their publication, however, Coker and co-workers[10] have performed a systematic study of the electronic states of I_3 using the semiempirical DIM (diatomics-in-molecules) method. This work indicated that I_3 has a centrosymmetric, weakly bound ground state with $\Omega = 1/2$. Simulations of the anion PES assuming transitions to this state were in reasonable agreement with the experimental data of Taylor *et al.*[6] In a more recent study,[11] the properties of this proposed ground state were explored further, and two low-lying excited states with $\Omega = 3/2$ were found which were close in energy to the excited states seen in the low-resolution spectrum obtained by Zanni *et al.*[9]

In this work, we investigate the low-lying excited states of I_3 radical with anion photoelectron spectroscopy at a lower photodetachment wavelength (213 nm) than was used previously. The new spectra reveal several electronically excited states of the I_3 radical at higher resolution than in previous work;[9] these states are further characterized through the measurement of photoelectron angular distributions. In addition, photodissociation from more highly excited states

[a)]Present address: Department of Chemistry and Biochemistry, University of California, Los Angeles, California 90095.
[b)]Present address: Department of Chemistry, University of Utah, Salt Lake City, Utah 84112.

of the I_3 radical is investigated with fast beam photofragment translational spectroscopy, in which a fast beam of I_3 is generated by photodetachment of mass-selected I_3^-. This work represents the first observation of electronic transitions in I_3. Photofragment mass and translational energy distributions were measured at several photolysis energies (4.59, 4.96, and 5.17 eV). Several dissociation channels are observed, including three-body dissociation of I_3.

II. EXPERIMENT

Two instruments, a negative ion photoelectron spectrometer and a fast radical beam photofragment translational spectrometer, are used for this study. To generate anions in both instruments, argon gas (3 psig) flows over iodine crystals (I_2) at room temperature. The resulting mixture supersonically expands through a pulsed valve into the source region of the apparatus. Anions were generated by a 1 keV electron beam, which crosses the expansion, and cooled to rotational temperatures of 30–50 K during expansion.

In the anion photoelectron spectrometer,[12,13] negative ions generated in the ion source pass through a skimmer into a differentially pumped region. They are extracted perpendicular to their flow direction by a pulsed electric field and injected into a linear reflectron time-of-flight (TOF) mass spectrometer[14,15] with a mass resolution ($m/\Delta m$) of 2000. The ion of interest is selectively photodetached using the fifth harmonic (213 nm, 5.822 eV) of a pulsed Nd:YAG laser.

The electron kinetic energy (EKE) distribution is determined by TOF analysis in a 1 m field-free flight tube. The energy resolution is 8–10 meV at 0.65 eV and degrades as $(\mathrm{EKE})^{3/2}$. The data in electron kinetic energy is converted to electron binding energy (EBE) by subtracting it from the photon energy. The EBE is given by Eq. (1) where EA is the adiabatic electron affinity and E^0 and E^- are the internal energies of the neutral and anion, respectively.

$$\mathrm{EBE}=h\nu-\mathrm{EKE}=\mathrm{EA}+E^0-E^-. \tag{1}$$

The photoelectron angular distribution is obtained through measurement of the photoelectron spectrum at two laser polarization angles, $\theta=0°$ and 90°, where θ is the angle between the electric field vector of the laser and the direction of election detection. The laser polarization is rotated with a half-wave plate. The angular dependence of the photodetachment intensity for polarized light and randomly oriented molecules is given by Eq. (2),[16]

$$\frac{d\sigma}{d\Omega}=\frac{\sigma_{\mathrm{total}}}{4\pi}\left[1+\frac{\beta(\mathrm{EKE})}{2}(3\cos^2\theta-1)\right], \tag{2}$$

where σ_{total} is the total photodetachment cross section and $\beta(\mathrm{EKE})$ is the anisotropy parameter ($-1\leqslant\beta\leqslant 2$). Each electronic state typically has a characteristic anisotropy parameter (β) and this can be used to distinguish peaks of overlapping electronic transitions. The anisotropy parameter of a peak can be calculated[17] using Eq. (3),

$$\beta=\frac{I_{0°}-I_{90°}}{\frac{1}{2}I_{0°}+I_{90°}}, \tag{3}$$

where $I_{0°}$ and $I_{90°}$ are the intensities of the peak taken at laser polarization angles $\theta=0°$ and 90°.

Photodissociation of the I_3 radical was studied using our fast radical beam photofragment translational spectrometer. In this instrument,[18,19] negative ions formed in the source region are accelerated to 8 keV and separated temporally by a TOF mass spectrometer. The I_3^- ion packet is intersected by a pulsed beam from KrF excimer laser (248 nm), photodetaching the anions to yield neutral I_3 radicals. Any remaining ions are removed by the application of an electrical deflection pulse. The I_3 radicals pass through a 1 mm diameter aperture and are then intersected by a linearly polarized pulsed dye laser beam, resulting in photodissociation of some of the radicals. Photodissociation was investigated at three wavelengths, 270, 250, and 240 nm, each of which was generated by frequency-doubling a fundamental wavelength at which the dye laser power was maximal. Note that at the photodetachment wavelength, 248 nm, photodissociation as well as photodetachment of I_3^- is expected. However, nearly all photofragments from I_3^- are blocked by the 1 mm aperture before the second laser.

Photofragments are detected by a coaxially mounted microchannel plate detector. A blocking strip across the center of detector prevents parent molecules from reaching the detector, whereas photofragments with sufficient recoil energy miss the beam block and strike the detector. These fragments are generally detected with high efficiency (up to 50%) due to their high laboratory kinetic energy.

In the photodissociation experiment, two photofragments from a parent molecule are collected in coincidence using a time- and position-sensitive detector at a fixed wavelength and the dissociation dynamics are investigated. We measure the distance R between the two fragments on the detector, the time difference τ of their arrival, and the individual displacements of the two fragments, r_1 and r_2, from the detector center for each dissociation event. From these we obtain the center-of-mass translational energy E_T, the scattering angle θ with respect to the laser polarization (parallel to the ion beam axis), and the photofragment mass ratio m_1/m_2 via

$$\frac{m_1}{m_2}=\frac{r_2}{r_1}\left(1-\frac{v_0\tau}{l}\right), \tag{4}$$

$$\theta=\tan^{-1}\left(\frac{R}{v_0\cdot\tau}\right), \tag{5}$$

$$E_T\cong E_0\cdot\frac{\mu}{M}\cdot\frac{(v_0\cdot\tau)^2+R^2}{l^2}. \tag{6}$$

Here E_0 and v_0 are the ion beam energy and velocity, respectively, μ is the reduced mass of the photofragments, and l is the flight length from the photodissociation region to the detector. Although the relative recoil distance R is determined with high precision ($R/\Delta R\approx 100$), the individual recoil distances r_1 and r_2 are less precisely determined due the finite size of the parent beam, resulting in $m/\Delta m\approx 10$. The energy resolution ($\Delta E_T/E_T$) under the conditions in these studies is around 2%. While only two particles per event can be analyzed using this coincidence detection scheme, we showed recently in a photodissociation study of the I_3^-

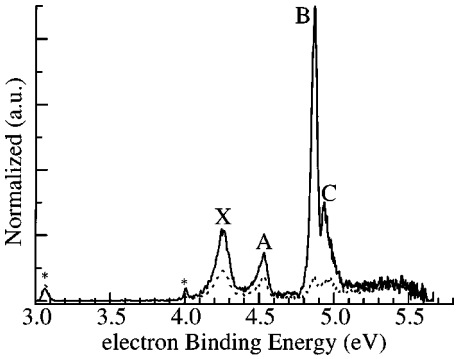

FIG. 1. Photoelectron spectrum of I_3^- anion at 5.822 eV taken at laser polarization angles $\theta=90°$ (solid line) and 0° (dotted line).

anion[20] that three-body dissociation could be unambiguously identified if one of the atoms strikes the beam block, a situation that appears to apply to neutral I_3 as well.

III. RESULTS AND ANALYSIS

A. Photoelectron spectrum of the I_3^- anion

Figure 1 shows anion photoelectron spectra of I_3^- taken at 213 nm (5.822 eV). These spectra, taken at two polarization angles, have been normalized with respect to laser shots to facilitate comparison of peak intensities. All features in the $\theta=90°$ spectrum (solid line) are much more intense than in the $\theta=0°$ spectrum (dotted line). The four main features are labeled as X, A, B, and C in the spectra. Two additional features labeled with an asterisk (*) are due to photodetachment of I^-, which is formed from the photodissociation of the parent I_3^- anion. Absolute peak positions and anisotropy parameters (β) for corresponding peaks are listed in Table I.

Peak X represents the transition to the electronic ground state of I_3, while peaks A–C are from transitions to excited states. Peaks B and C were not observed in the previously reported photoelectron (PE) spectrum at the lower photon energy of 4.657 eV (266 nm).[6] Although peak X showed resolved vibrational structure in the 266 nm spectrum, no such structure is seen in Fig. 1 because the electron energy resolution drops with increasing electron kinetic energy. Peak A shows no vibrational structure at either photodetachment wavelength, and the additional features at 213 nm, B and C, do not exhibit vibrational structure either.

We first consider the assignment of peaks X and A. The ground state molecular orbital configuration for the I_3^- anion is $\cdots(\sigma_u)^2(\pi_u)^4(\pi_g)^4(\sigma_g)^2(\pi_u^*)^4$.[21] From Koopman's theorem, the ground state of I_3 is accessed by removal of an electron from the highest occupied molecular orbital, leaving an I_3 radical in either of two $^2\Pi_u$ spin–orbit states, $^2\Pi_{u,3/2}$ and $^2\Pi_{u,1/2}$, with the $\Omega=3/2$ level being lower in energy. In addition, the similar anisotropy parameters for peaks X and A in Table I suggest that photoelectrons for these two features might be removed from the same orbital of I_3^-. These considerations support assignments of peaks X and A to the $^2\Pi_{u,3/2}$ and $^2\Pi_{u,1/2}$ states, respectively, of I_3 in agreement with the state-ordering of the isovalent species XeF_2^+.[22,23]

However, at 266 nm, the anisotropy parameters for peaks X and A were found to be 0.24 and −0.21 (these were misreported in the previous article), so the agreement of the β values at 213 nm may be fortuitous and not be a strong indication that the two peaks result from detachment out of the same orbital. This would be consistent with a relativistic extended Huckel calculation on I_3 by Pyykkö[24] which predicts a $^2\Pi_{u,3/2}$ ground state and a low-lying $^2\Sigma_g^+$ excited state from detachment of a σ_g electron; this state ordering results from the large spin–orbit splitting in I_3 raising the $^2\Pi_{u,1/2}$ state above the $^2\Sigma_g^+$ state.

In the highest level calculations on I_3 published to date, a different assignment is proposed. The DIM calculations by Margulis *et al.*[10,11] find the ground state of I_3 to have $\Omega=1/2$, where Ω is the projection of total angular momentum on the molecular axis. In their calculation, I_3 was assumed to be linear. Although there was no discussion of the molecular orbital configuration, this state presumably results from detachment of a σ_g electron from I_3^-. The calculated dissociation energy of this state, 0.19 eV, agrees with experiment[6,7] (0.14 ± 0.06 eV) and the calculated symmetric stretch frequency, 126 cm^{-1}, is close to the experimental value of 115 ± 5 cm^{-1}. Margulis *et al.* find the first excited state to be a $\Omega=3/2$ state, which should be the lower spin–orbit state resulting from detachment of a π_u^* electron. This state is calculated to lie 0.13 eV above the ground state, smaller than the X–A splitting of 0.27 eV but close enough to be a viable assignment. The assignment of peaks X and A based on the DIM calculations is also consistent with the assignment of the Cl_3^- photoelectron spectrum,[25] in which the lowest two (overlapped) transitions were assigned to the $^2\Sigma_g^+$ and $^2\Pi_u$ states of Cl_3. While the agreement between the DIM calculations and experiment appears convincing, very recent *ab initio* calculations by Kaledin and Morokuma[26] find the ground state of I_3 to be bend with a small (0.1 eV) barrier to linearity, and that $\Omega=3/2$ for this state in its linear geometry. At this point, the assignment of peaks X and A is not definitive, but it is reasonable to assume that one is due to the $\Omega=3/2(^2\Pi_{u,3/2})$ state and the other to the $\Omega=1/2(^2\Sigma_g^+)$ state.

Peaks B and X are separated by 0.615 eV. Margulis and Coker[11] calculate the second excited state of I_3 to be a $\Omega=3/2$ state lying 0.67 eV above the I_3 ground state, again in reasonable agreement with experiment. This neutral state should correspond to the lower spin–orbit state resulting from detachment of a π_g electron from I_3^-. Peak C, lying 0.064 eV (516 cm^{-1}) above peak B, is more problematic. Coker finds the antisymmetric stretch frequency to be 416 cm^{-1} for the $\Omega=3/2$ state, and his simulation of the photoelectron spectrum suggests that peak C involves transitions to vibrationally excited levels of this state in which the anti-

TABLE I. Peak position and anisotropy parameter (β) for feature in the I_3^- photoelectron spectrum.

Peak	Position (eV)	Anisotropy parameter (β)	Splitting from the origin of $\tilde{X}$ state of I_3 (eV)
X	4.254	−0.48	0.028
A	4.533	−0.41	0.307
B	4.869	−0.88	0.643
C	4.933	−0.69	0.707

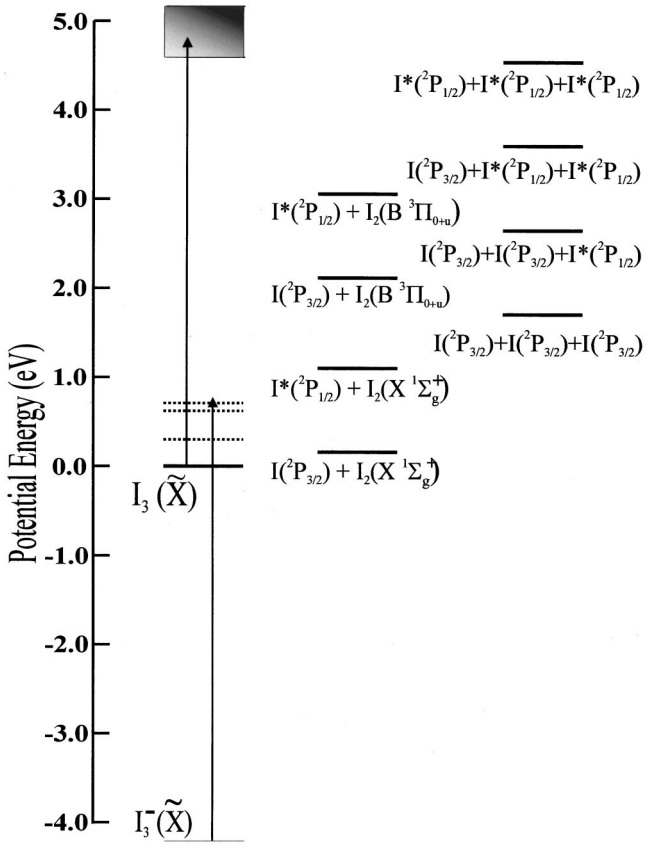

FIG. 2. Energetics of I_3. The three excited states of I_3 observed in our PES spectra are shown as dotted lines.

symmetric stretch is singly excited. However, the calculated 416 cm^{-1} frequency seems very high, given that the vibrational frequency of the I_2 ground state is only 213 cm^{-1}. In addition, if the anion and neutral are centrosymmetric (as predicted by the calculation), then transitions to singly excited antisymmetric stretch levels have Franck–Condon factors of zero. It seems more likely that peak C is a transition to a third excited state, possibly the $\Omega=1/2$ spin–orbit state from detachment of a π_u^* electron, rather than a vibrationally excited level of the second excited $\Omega=3/2$ state. This assignment is also supported by the different anisotropy parameters of peaks B and C (Table I).

Figure 2 shows the energy of the I_3 ground state and the three excited states seen in the PES relative to I_3^- and the various I_3 fragmentation channels, using the dissociation energy of I_3 and the well-known energetics of I_2 and I.[27,28] Only the ground state of I_3 is thermodynamically stable with respect to the lowest energy product channel, $I(^2P_{3/2})+I_2(X\,^1\Sigma_g^+)$.

B. Photodissociation of the I_3 radical

Photodissociation dynamics experiments on I_3 were carried out at three photolysis energies: 4.59, 4.96, and 5.17 eV. In this experiment, the I_3 radical is generated by photodetaching the I_3^- anion. For most systems studied on this instrument, the photodetachment energy is chosen to be close enough to the detachment threshold that only radicals in their vibrational ground state are produced. However, the PES of

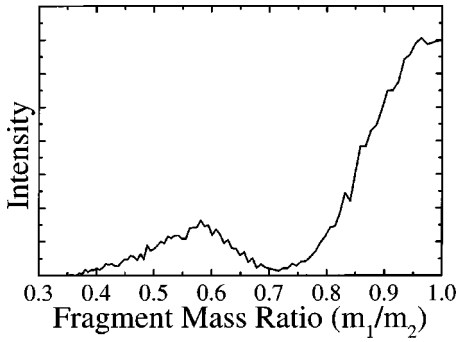

FIG. 3. Photofragment mass ratio (m_1/m_2) of I_3 at a photolysis energy of 4.59 eV (270 nm).

I_3^- shows an extended progression in a low frequency vibration,[6] indicating a small Franck–Condon factor between the anion and neutral vibrational ground states. Under these circumstances, selective population of the $v=0$ neutral level is in principle possible by detachment just above threshold, but in practice one cannot produce sufficient I_3 to carry out the experiment. Instead, we detach at 5.00 eV (248 nm), well above the energy needed to populate the entire ground state Franck–Condon envelope of vibrational levels as well as the three excited states seen in the 213 nm photoelectron spectrum. As shown in Fig. 2, the excited states lie well above the lowest $I+I_2$ asymptote, and we assume they dissociate in the 10 μs delay between the detachment and dissociation pulses. Thus, we expect our photodissociation experiment to involve excitation from only the ground electronic state of I_3.

1. Photofragment mass ratio (m_1/m_2)

For each dissociation event, the mass ratio of the photofragments is determined using Eq. (4). In Fig. 3, the fragment mass ratio obtained at the photolysis energy of 4.59 eV shows that there are two rather broad peaks peaking at photofragment mass ratios of 0.6 and 1.0. The peak at 0.6 is assigned to products with a 1:2 mass ratio; the deviation from the expected value of 0.5 may result from a combination of poor photofragment mass resolution and stepwise three-body dissociation (see below). Similar mass distributions are seen at the other two energies.

As shown in Fig. 2, there are several product channels that are energetically accessible at our photolysis energies:

$$I_3(\tilde{X})+h\nu_{\text{photon}} \rightarrow I(^2P_{3/2})+I_2(X\,^1\Sigma_g^+) \qquad D_0=0.14\pm0.06\ \text{eV (channel 1)},$$

$$I^*(^2P_{1/2})+I_2(X\,^1\Sigma_g^+) \qquad D_0=1.08\pm0.06\ \text{eV (channel 2)},$$

$$I(^2P_{3/2})+I_2(B\,^3\Pi_{0_u^+}) \qquad D_0=2.10\pm0.06\ \text{eV (channel 3)},$$

$$I^*(^2P_{1/2})+I_2(B\,^3\Pi_{0_u^+}) \qquad D_0=3.04\pm0.06\ \text{eV (channel 4)},$$

$$I(^2P_{3/2}) + I(^2P_{3/2}) + I(^2P_{3/2})$$
$$D_0 = 1.69 \pm 0.06\ \text{eV (channel 5)},$$
$$I^*(^2P_{1/2}) + I(^2P_{3/2}) + I(^2P_{3/2})$$
$$D_0 = 2.63 \pm 0.06\ \text{eV (channel 6)},$$
$$I^*(^2P_{1/2}) + I^*(^2P_{1/2}) + I(^2P_{3/2})$$
$$D_0 = 3.57 \pm 0.06\ \text{eV (channel 7)},$$
$$I^*(^2P_{1/2}) + I^*(^2P_{1/2}) + I^*(^2P_{1/2})$$
$$D_0 = 4.51 \pm 0.06\ \text{eV (channel 8)}.$$

The low-lying, weakly bound $A'\,^3\Pi_{2u}(T_e = 1.245\ \text{eV})$[29] and $A\,^3\Pi_{1u}(T_e = 1.352\ \text{eV})$[30] excited states of I_2 are also accessible. However, we cannot distinguish I (or I*) + $I_2(A'\,^3\Pi_{2u}$ and $A\,^3\Pi_{1u})$ from I (or I*) + vibrationally excited I_2 in the X state in our $P(E_T)$ distributions.

Channels 1–4 are two-body dissociation channels yielding photofragments with mass ratio 1:2. Channels 5–8 are three-body dissociation channels. These are more problematic, in principle, because the coincidence detector can detect at most two fragments per dissociation event. However, if the I_3 radicals undergo symmetric (concerted) three-body dissociation, the two end atoms fly apart at approximately equal and opposite center-of-mass (CM) velocities, while the central atom remains stationary in the CM frame. It therefore follows the same trajectory of the parent molecule and will hit the beam block in front of the detector. As a result, symmetric three-body dissociation of I_3 will appear as a two-body channel with a mass ratio of 1:1 in our experiment. Hence, our observation of products with a 1:1 mass ratio implies that symmetric three-body dissociation of I_3 occurs. Similar product mass distributions and assignments were seen in a photodissociation experiment of I_3^- performed on the same instrument.[20]

2. Energy and angular distributions

For each mass channel, the joint translational energy and angular distribution is given by

$$P(E_T, \theta) = P(E_T) \cdot (1 + \beta(E_T) \cdot (3\cos^2\theta - 1)/2). \qquad (7)$$

Here, E_T is the translational energy release, θ is the angle between the photofragment recoil velocity vector and the laser polarization (parallel to the ion beam axis), and $\beta(E_T)$ is the anisotropy parameter. For the channel with mass ratio 1:1, $\mu = 1/2\ m_I$ (m_I = mass of I atom) in Eq. (6) as discussed previously.[20] The limiting cases of $\sin^2\theta$ and $\cos^2\theta$ angular distributions are given by $\beta = -1$ and $+2$, respectively. Generally speaking, a parallel transition yields $\beta > 0$, whereas $\beta < 0$ for a perpendicular transition.

We find $\beta > 0$ for both mass channels, suggesting that the electronic transition is a parallel transition with $\Delta\Omega = 0$. A more precise measurement of β is hampered because much of the photofragment signal occurs at $E_T > 1.5$ eV (see below) for which the angular acceptance of the detector is quite low.[31]

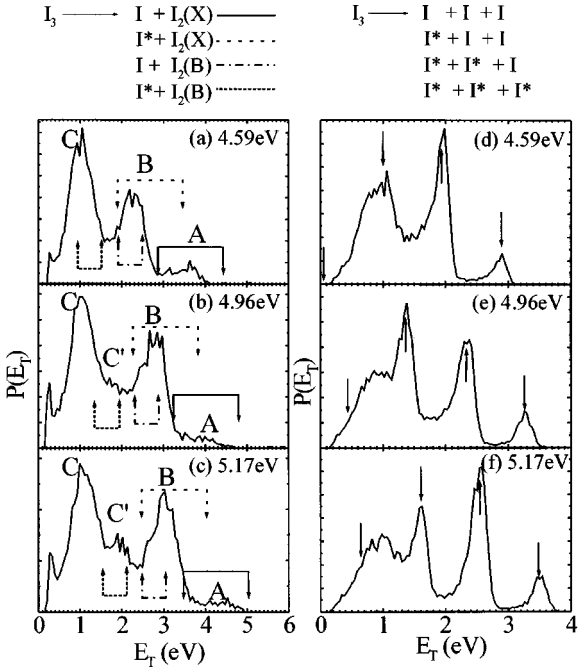

FIG. 4. Translational energy $P(E_T)$ distributions of I_3 at photolysis energies at 4.59, 4.96, and 5.17 eV: (a)–(c) with 1:2 mass ratio and (d)–(f) with 1:1 mass ratio. The arrows indicate the allowed energies for the three-body channels assuming concerted dissociation.

3. 1:2 mass channel

$P(E_T)$ distributions for products with mass ratio 1:2 are shown in Figs. 4(a)–4(c). At the lowest excitation energy (4.59 eV), three features labeled as A, B, and C in Fig. 4(a) are visible. As the photon energy increases, feature C remains at the same E_T while features A and B shift to higher E_T. In addition, at the two higher photon energies, another feature labeled as C' in Figs. 4(b)–4(c) appears between features B and C.

Channels 1–4 are energetically possible at each excitation energy in Fig. 4. The four brackets in each plot show the maximum and minimum translational energies for channels 1–4; at energies below the minimum, the I_2 internal energy exceeds its bond dissociation energy and it would dissociate long before reaching the detector. At all three energies, feature A fits within the allowed translational energy range for channel 1, so we assign it to this channel. Similar considerations indicate that feature B is due to a combination of channels 2 and 3; these cannot be completely distinguished because their allowed energy ranges are strongly overlapped. However, in Figs. 4(b) and 4(c) some of feature B extends beyond the maximum E_T for channel 3, so at least some of this feature is from channel 2. At the two higher excitation energies (4.96 and 5.17 eV), feature C′ can be assigned as channel 4, $I^* + I_2(B)$. At the lowest energy it is not clear if this channel is present because of strong overlap of the allowed translational energy range with the large low-energy feature C. Note that the radiative lifetime of the $I_2(B)$ state is in the range of 0.7–2 μs,[32] depending on vibrational level, which is considerably shorter than the flight time from the interaction region to the detector (17 μs). Hence the I_2 product associated with channels 3 and 4 fluoresces to the ground

state before it is detected; this of course has no effect on the translational energy release.

The assignment of feature C is problematic, because there is no stable I_2+I channel in this energy range. Since peak C lies just below the minimum energy for $I^*+I_2(B)$, it may result from I^*+I_2 formed in its $B\,^3\Pi_{0_u^+}$ state with enough energy (>0.53 eV) to dissociate to $I+I^*$. This represents an example of stepwise (asynchronous) three-body dissociation, in which the two I_3 bonds break on different time scales, i.e.,

$$I_3 \underset{(a)}{\rightarrow} I^* + I_2(B) \underset{(b)}{\rightarrow} I^* + I + I^*. \tag{8}$$

$I_2(B)$ excited above its dissociation limit will survive for at most one vibrational period, but this should be sufficient for the two steps to be considered as distinct. In contrast to symmetric three-body dissociation, the stepwise mechanism poses problems for our detection scheme because it is more likely to lead to dissociation events in which all three particles hit the detector, and we can only process two particles per dissociation event. However, if these two particles are the I^* from (a) and one of the atomic fragments from dissociating $I_2(B)$, analysis of the coincidence data should yield a translational energy representing the relative translational energy between the two fragments from (a), but broadened because of the energy released from dissociation of the highly excited $I_2(B)$. One problem with this mechanism is that one would expect peak C to shift toward higher E_T as the photon energy is raised, but no shift is observed. We therefore regard this mechanism for peak C as tentative. While it is also possible that peak C comes from predissociation of bound levels of the $I_2(B)$ state, this is less likely because predissociation from the B state is generally a minor channel compared to fluorescence, although it can be competitive with fluorescence at very high J levels ($J>100$).[32]

4. 1:1 mass channel

Figures 4(d)–4(f) show the $P(E_T)$ distributions for the 1:1 mass channel. These distributions show several relatively sharp peaks along with a broad feature around $E_T=1.0$ eV. The assignment of the sharp features is straightforward. At each photon energy, concerted three-body dissociation to three I atoms, in which the central I atom has no translational energy in the center-of-mass frame of reference, yields a single value of allowed translational energy for each of the channels 5–8. The allowed energies are indicated by the arrows in Figs. 4(d)–4(f), and each sharp peak (but not the broad, low energy peak) is centered at one of these energies. This agreement provides further proof that the three-body dissociation is concerted and that dissociation is occurring from a linear (or at least quasilinear), centrosymmetric species. We see that channels 5 and 6 are active at each excitation energy. Channel 7 is clearly observed at $h\nu \geqslant 4.96$ eV and channel 8 is not evident at any of the energies we studied.

While the sharp peaks in Figs. 4(d)–4(f) correspond to the appropriate kinetic energies for concerted three-body dissociation, they are considerably broader than the experimental kinetic energy resolution, ~300 meV vs ~20 meV. Similar results were seen in three-body dissociation from I_3^-,[20] in which peaks were observed at exactly the right energies but were ~150 meV wide. Trajectory calculations run for I_3^- dissociation[20] indicated that the additional width resulted from deviation of the three-body trajectories from the symmetric stretch coordinate, so that the central atom was not always halfway between the two end atoms at the detedctor. The further broadening of the three-body features from I_3 dissociation (i.e., 300 vs 150 meV) most likely reflects the initial internal energy spread of the I_3 radicals since the entire Franck–Condon envelope of vibrational levels is populated by photodetachment in this experiment (see above).

We next consider the broad, low energy feature that appears around 1 eV in the $P(E_T)$ distributions. This feature does not correspond to an allowed energy for concerted three-body dissociation and therefore must have another origin. This peak occurs in the same energy range as peak C in the distributions for the 1:2 mass channel and we tentatively assign it to the same origin, namely stepwise three-body dissociations via Eq. (8). Some of these events will be counted as products with mass ratio 1:1, as long as the measured value of $m_1/m_2>0.7$ [see Eq. (4) and Fig. 3] for the two detected photofragments. We note that I_2 has a multitude of low-lying, repulsive electronic states, and cannot rule out that the production of I_2 in one or more of these states also contributes to the intensity of the low energy feature or to the broadening of the sharper features in Figs. 4(d)–4(f). A more detailed understanding of three-body channels other than concerted dissociation requires a detector that can process three or more particles per dissociation event; such a detector is currently under development in our laboratory.

IV. DISCUSSION

The anion photoelectron spectrum of I_3^- presented here shows transitions to the ground and three low-lying excited states of I_3. The presence of these low-lying excited states is of interest in light of electronic quenching experiments on I^* performed in several laboratories. The primary quenching mechanism is through collisions with I_2, i.e., $I^*+I_2 \rightarrow I+I_2$. The large rate constant and negligible activation energy observed for this reaction led Leone, Houston, and their co-workers[3–5] to postulate that the reactants form a short-lived, electronically excited I_3 complex that dissociates to $I+I_2$ by a nonadiabatic transition. As shown in Fig. 2, all three excited states seen in the anion photoelectron lie below the I^*+I_2 asymptote and are therefore possible candidates for the reactive intermediate in the electronic quenching reaction. The specific identification of the state or states that are involved requires a more definitive assignment of these states than is currently available.

The identity of the excited electronic state(s) accessed in the I_3 photodissociation experiments remains undetermined. However, several trends in the photofragment energy and angular distributions are noteworthy. At each photon energy, the anisotropy parameter is positive, indicating the transition moment is parallel and that Ω is unchanged upon excitation. In addition, the $P(E_T)$ distributions for the 1:2 and 1:1 mass channels are quite similar in appearance at each energy, sug-

gesting that the same state or manifold of states is accessed from 4.59–5.17 eV. Most of the features in the $P(E_T)$ distributions shift toward higher kinetic energy as the photon energy is raised, reflecting the increased available energy for each product channel. In the distributions for 1:2 products, the kinetic energy distributions for each channel cover a good bit of the allowed energy range for that channel, indicating that there is significant vibrational and rotational excitation of the I_2 fragment regardless of its electronic state. Finally, although it is difficult to calculate quantitative branching ratios because many of the product channels overlap, formation of ground state products is disfavored. In the 1:2 distributions, feature A corresponding to $I+I_2$ is considerably weaker than features corresponding to excited I and/or I_2, while in the three-body distributions the I+I+I channel is weaker than I^*+2I or $2I^*+I$.

The results presented here represent the first experimental study of the spectroscopy and dynamics of excited electronic states in I_3. The detailed interpretation of our results certainly requires more theoretical work on the relevant potential energy surfaces. We hope the results presented here will stimulate more experimental and theoretical investigations of this important chemical species.

ACKNOWLEDGMENTS

This research is supported by the Air Force Office of Scientific Research under Grant No. F49620-00-1-0145. The authors thank Dr. Arthur Suits for loaning the KrF excimer laser used in this study.

[1] D. L. Bunker and N. Davidson, J. Am. Chem. Soc. **80**, 5090 (1958).
[2] V. I. Balykin, V. S. Lektokhov, V. I. Mishin, and V. A. Semchishen, Chem. Phys. **17**, 111 (1976).
[3] G. E. Hall, W. J. Marinelli, and P. L. Houston, J. Phys. Chem. **87**, 2153 (1983).
[4] H. Hofmann and S. R. Leone, J. Chem. Phys. **69**, 641 (1978).
[5] J. I. Cline and S. R. Leone, J. Phys. Chem. **95**, 2917 (1991).
[6] T. R. Taylor, K. R. Asmis, M. T. Zanni, and D. M. Neumark, J. Chem. Phys. **110**, 7607 (1999).
[7] K. Do, T. P. Klein, C. A. Pommerening, and L. S. Sunderlin, J. Am. Soc. Mass Spectrom. **8**, 688 (1997).
[8] M. T. Zanni, B. J. Greenblatt, A. V. Davis, and D. M. Neumark, Proc. SPIE **3271**, 196 (1998).
[9] M. T. Zanni, B. J. Greenblatt, A. V. Davis, and D. M. Neumark, J. Chem. Phys. **111**, 2991 (1999).
[10] C. J. Margulis, D. A. Horner, S. Bonella, and D. F. Coker, J. Phys. Chem. A **103**, 9552 (1999).
[11] C. J. Margulis and D. F. Coker, J. Chem. Phys. (submitted).
[12] R. B. Metz, A. Weaver, S. E. Bradforth, T. N. Kitsopoulos, and D. M. Neumark, J. Phys. Chem. **94**, 1377 (1990).
[13] C. Xu, G. R. Burton, T. R. Taylor, and D. M. Neumark, J. Chem. Phys. **107**, 3428 (1997).
[14] B. A. Mamyrin and D. V. Shmikk, Zh. Eksp. Teor. Fiz. **49**, 762 (1979).
[15] G. Markovich, R. Giniger, M. Levin, and O. Cheshnovsky, J. Chem. Phys. **95**, 9416 (1991).
[16] J. Cooper and R. N. Zare, in *Lectures in Theoretical Physics*, edited by S. Geltman, K. T. Mahanthappa, and W. E. Brittin (Gordon and Breach, New York, 1969), Vol. XI-C, p. 317.
[17] K. M. Ervin and W. C. Lineberger, in *Advances in Gas Phase Ion Chemistry*, edited by N. G. Adams and L. M. Babcock (JAI, Greenwich, 1992), Vol. 1, p. 121.
[18] D. R. Cyr, R. E. Continetti, R. B. Metz, D. L. Osborn, and D. M. Neumark, J. Chem. Phys. **97**, 4937 (1992).
[19] R. E. Continetti, D. R. Cyr, R. B. Metz, and D. M. Neumark, Chem. Phys. Lett. **182**, 406 (1991).
[20] H. Choi, R. T. Bise, A. A. Hoops, and D. M. Neumark, J. Chem. Phys. **113**, 2255 (2000).
[21] T. Okada and J. Hata, Mol. Phys. **43**, 1151 (1981).
[22] C. R. Brundle, M. B. Robin, and G. R. Jones, J. Chem. Phys. **52**, 3383 (1970).
[23] B. W. Yates, K. H. Tan, G. M. Bancroft, L. L. Coatsworth, J. S. Tse, and G. J. Schrobilgen, J. Chem. Phys. **84**, 3603 (1986).
[24] A. Viste and P. Pyykkö, Int. J. Quantum Chem. **25**, 223 (1984).
[25] A. L. Kaledin, M. C. Heaven, K. Morokuma, and D. M. Neumark, Chem. Phys. Lett. **306**, 48 (1999).
[26] A. Kaledin and K. Morokuma (private communication).
[27] K. P. Huber and G. Herzberg, *Molecular Spectra and Molecular Structure. IV. Constants of Diatomic Molecules* (Van Nostrand Reinhold Co., New York, 1979).
[28] S. Bakin and J. O. Stoner, Jr., *Atomic Energy Level and Grotrian Diagrams Vol. 2* (North-Holland, New York, 1978).
[29] X. N. Zheng, S. L. Fei, M. C. Heaven, and J. Tellinghuisen, J. Chem. Phys. **96**, 4877 (1992).
[30] D. R. T. Appadoo, R. J. Leroy, P. F. Bernath, S. Gerstenkorn, P. Luc, J. Verges, J. Sinzelle, J. Chevillard, and Y. Daignaux, J. Chem. Phys. **104**, 903 (1996).
[31] D. R. Cyr, Ph.D. thesis, University of California, Berkeley, 1993.
[32] J. Vigue, M. Broyer, and J. C. Lehmann, J. Phys. (Paris) **42**, 949 (1981).